ChemComm

Cite this: *Chem. Commun.*, 2011, **47**, 11957–11959

www.rsc.org/chemcomm

COMMUNICATION

Breakthrough in concentration quenching threshold of upconversion luminescence *via* spatial separation of the emitter doping area for bio-applications†

Xiaomin Liu,[a] Xianggui Kong,*[a] Youlin Zhang,[a] Langping Tu,[a] Yu Wang,[b] Qinghui Zeng,[a] Chunguang Li,[c] Zhan Shi[c] and Hong Zhang*[b]

Received 2nd August 2011, Accepted 14th September 2011
DOI: 10.1039/c1cc14774a

The concentration quenching threshold of upconversion luminescence was broken through for the first time *via* a designed strategy: spatial separation of the emitter doping area.

Rare-earth ion-doped luminescence upconversion (UC) nanoparticles have attracted much attention in recent years due to their superior spectroscopic properties that mainly arise from the existence of stable intermediate states, which may result in their potential applications in many fields, especially in biology/biomedicine.[1] Among these materials, hexagonal-phase $NaYF_4$ has been reported as one of the most efficient hosts for performing infrared-to-visible photon conversion in the doped rare-earth ions.[2] However, considering the inherent requirement of a low excitation density level in biological systems, enhancing the UC intensity is a challenge to these photonic nanoparticles due to their low efficiency, which has never been higher than several percent.[3]

As is well-known, the luminescence intensity mainly depends on two factors: (i) the properties of the individual luminescence centers and (ii) the number of the luminescence centers (emitters). In order to increase the UC intensity, researchers have, as far as UC nanomaterials are concerned, been focused on point (i), *i.e.* how to minimize the quenching centers and channels. Successful approaches to achieve this include (1) adding an active/inert shell to the doped core,[4–6] (2) improving the synthetic routes[2f] and (3) using external factors, *e.g.* utilizing the interactions between the luminescence centers and metal particles,[7] but the success of all of these efforts is limited by the low doping level of the emitters in the nanoparticles. The most effective way to enhance the UC intensity is by increasing the number of emitters (point (ii)). However, high doping levels of the emitters lead to deleterious resonant energy transfer, resulting in quenching of excitation energy.[8] It has been proven and is well-accepted that the optimal dopant concentration is approximately 2 mol% for emitter Er^{3+}, as far as UC nanomaterial $NaYF_4$:Yb^{3+}, Er^{3+} is concerned,[9] and no effort has yet been reported on the breakthrough of this limitation. In this work, we have broken through the well-accepted upper limit of the concentration quenching threshold, *e.g.* from ~2 mol% to 5 mol% for Er^{3+}, by a designed strategy of spatial separation of the emitter doping area (Fig. 1(b)), in which the separating layer effectively minimizes the energy transfer between the emitters in the inside and outside layers and largely lowers the possibility of trapping of excitation energy by defects, resulting in an enhancement of the UC intensity, which is also significant in biomedical application, *e.g.* singlet oxygen generation becomes more efficient. Furthermore, this approach may apply to a wide range of photonic doping systems.

The architecture, with the emitter doping area spatially separated (Fig. 1(b)), was an extension of the core/active shell structure (Fig. 1(a)), which has been intensively studied and proven to effectively enhance the UC intensity.[5,6] However, the optimal dopant concentration is still 2 mol% for emitter Er^{3+} in the core/active shell structure and this is difficult to increase due to concentration quenching.[5]

The nanoparticle of the designed approach (denoted as model A) was synthesized using the well-known thermolysis process *via* decomposition of metal trifluoroacetate precursors (see ESI for the complete synthetic approach†). The resulting hexagonal-phase nanoparticles had an average particle size of

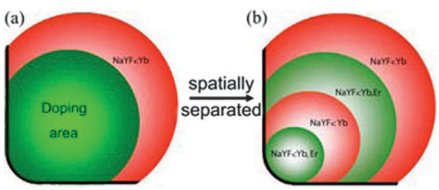

Fig. 1 (a) The classical core/active shell structure. (b) The designed strategy with emitters doping area spatially separated. It contains four parts: the core ($NaYF_4$:Yb^{3+}, Er^{3+}), the first separating shell ($NaYF_4$:Yb^{3+}), the second illuminating shell ($NaYF_4$:Yb^{3+}, Er^{3+}) and the final active shell ($NaYF_4$:Yb^{3+}).

[a] *Changchun Institute of Optics, Fine Mechanics and Physics, Chinese Academy of Sciences, P. R. China. E-mail: xgkong14@ciomp.ac.cn*
[b] *Van't Hoff Institute for Molecular Sciences, University of Amsterdam, The Netherlands. E-mail: h.zhang@uva.nl*
[c] *State Key Laboratory of Inorganic Synthesis & Preparative Chemistry, College of Chemistry, Jilin University, P. R. China*

† Electronic supplementary information (ESI) available: Detailed experimental procedures, TEM images, XRD, UC luminescence and detailed spectra. See DOI: 10.1039/c1cc14774a

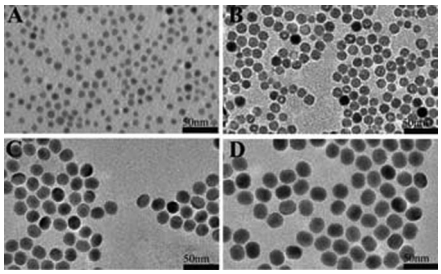

Fig. 2 TEM images of the different structured nanoparticles: (a) core; (b) with separating shell outside (a); (c) with illuminating shell outside (b); (d) with final active shell outside (c).

25 nm. The core-only nanoparticles had a mean particle diameter of 10 nm. The first separating shell, second illuminating shell and final active shell led to the size of the nanoparticles to be 15 nm, 20 nm and 25 nm respectively (see Figs 2 and S1–S3†). During the course of the shell preparation, the synthesis was performed using a mechanical pump for the precise addition of the shell precursors to the reaction vessel to eliminate any variation caused by the rate of addition. Thus, the observed increase in the size of the nanoparticles was attributed to the gradual growth of the shell around the core. From the difference in the particle sizes of these four structures, each shell thickness was estimated to be about 2.6 nm.

To further illustrate the existence of the emitter spatially separated architecture and the advantage over the traditional core–shell structure, two different models B and C with doping emitters homogeneously distributed were designed for control (see Figs S4 and S5†). As shown in the insets of Fig. 3(1), model A is the as-designed architecture; model B is a mimic of the situation where the structure of model A does not form and emitters Er^{3+} are diffused to the separating layer; model C is the classical core/active shell architecture, which exhibits the strongest UC luminescence up to now.[5]

Fig. 3(1) shows the corresponding UC emission spectra of the three different nanoparticles dispersed in cyclohexane with the same particle size and concentration (1 mg ml^{-1}), which reflect the luminescence of a single particle of the three models on an average level. In all cases, the UC emission was observed in the green and red spectral regions. The green emission at 510–570 nm is well-known and ascribed to transitions from the $^2H_{11/2}$ and $^4S_{3/2}$ excited states to the $^4I_{15/2}$ ground state (centered at 525 and 550 nm, respectively). The red emission between 630–680 nm is from the $^4F_{9/2}$ excited state to the ground state.[8]

The UC spectra also reveal distinct differences between these three models. The most obvious one seems to be the emission intensity. The highest emission is observed in model A by a factor of approximately 3.5 in the green and 2.3 in the red compared to model B, and by a factor of 2.1 in the green and 1.1 in the red compared to model C. It was mentioned above that model B is simply another structure of model A, where the doping emitters are homogeneously distributed. If Er^{3+} ions are not spatially separated in model A, the spectra of A and B would be similar, but Fig. 3(1) shows just the opposite. This result verifies the formation of model A (see Fig. S6†for further evidence). Models B and C have similar architecture with the emitters homogeneously distributed in the core, while the Er^{3+} concentration is less in model B (1.4%) than in model C (2%). In principle, the

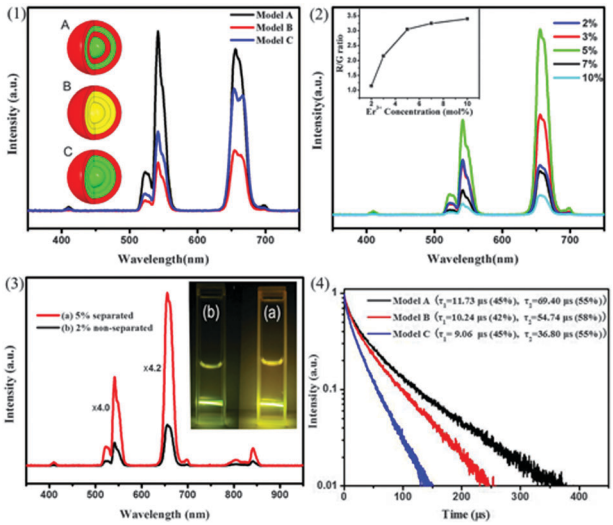

Fig. 3 (1) The UC PL spectra of colloidal nanocrystals with model A (black line), model B (red line) and model C (blue line). Insets are the structures of models A–C; (2) The UC PL spectra of colloidal $NaYF_4$ nanocrystals with model A co-doped with 20% Yb^{3+} and various concentrations of Er^{3+} ions (2–10%) with the R/G ratio shown in the inset; (3) The UC PL spectra of colloidal $NaYF_4$ nanocrystals with (a) model A doped with 5% Er^{3+} ions and (b) model C doped with 2% Er^{3+} ions. The inside picture shows the relative photographs of colloidal solutions of (a) and (b). All of the solutions detected for UC PL spectra were dispersed in cyclohexane (1 mg ml^{-1}) under 15 W cm^{-2} continuous excitation at 980 nm; (4) The decay curve of models A–C under 488 excitation.

growth of the emitter doping concentration would lead to an increase in the R/G (red to green) ratio,[10] which is substantiated by comparing the R/G ratio of models B (R/G ratio = 1.70) and C (R/G ratio = 2.15). It is also well-known that a high doping level can lead to deleterious resonant energy transfer, increasing the possibility of the excitation energy being trapped by quenching centers. This is indeed proved by further increasing the doping level of model C to 3%, where the concentration quenching happened (see Fig. S7†), in line with a previous report.[6] However, for model A, where the doping emitters are spatially separated, the overall upconversion luminescence is the strongest of the three models and the R/G ratio (R/G ratio = 1.15) is the lowest when the Er^{3+} concentration is 2 mol% (see Fig. S8† for further explanation). This is a promising sign that the as-designed model A may have the capacity to contain more emitters without concentration quenching.

To validate this hypothesis, we gradually increased the doping quantity of the Er^{3+} ions. Fig. 3(2) shows the UC PL spectra of colloidal $NaYF_4$ nanocrystals co-doped with Yb^{3+} (20%) and various concentrations of emitter Er^{3+} ions (2, 3, 5, 7 and 10%). The accuracy in determining the quantity of the doping Er^{3+} ions was guaranteed by EDS spectra, given in the supporting information (Fig. S9†), where yttrium, ytterbium, fluorine, sodium and erbium atoms were clearly detected in these samples. Furthermore, the Er^{3+} concentration in these samples was consistent with the doping quantity.

In Fig. 3(2), the highest intensities of the green and red emissions are observed at 5 mol%. When the concentration of Er^{3+} ions increases to over 5 mol%, the distance between

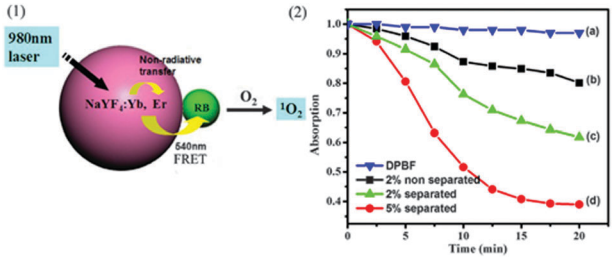

Fig. 4 (1) A schematic drawing of the FRET-based $NaYF_4$–Rose Bengal (UCP–RB) nanoconjugates. (2) The decay curves of the absorption of DPBF at 410 nm caused by (a) DPBF solution, (b) 2% Er^{3+} doped non-separated UCP–RB conjugates, (c) 2% Er^{3+} doped separated UCP–RB conjugates and (d) 5% Er^{3+} doped separated UCP–RB conjugates in ethanol as a function of irradiation time. The excitation wavelength is 980 nm.

Er^{3+}–Er^{3+} becomes so close that the concentration quenching is obvious, leading to the intensity dropping down at, *e.g.* 7 mol% and 10 mol%, respectively. Simultaneously, the red emission grows faster than the green one. The 2 mol% sample has a R/G ratio of 1.15. As the doping concentration increases, the red component becomes more prominent. For example, for the 3 mol% and 5 mol% samples, the ratio becomes 2.25 and 3.05, respectively. In addition, the upconversion luminescence of model A doped with 5 mol% Er^{3+} ions is approximately 4 times higher in intensity compared to that of model C doped with 2 mol% Er^{3+} ions, which has the strongest UC PL (see Fig. 3(3)). It is, therefore, evident that the emitter doping area spatial separated approach can indeed improve the threshold of concentration quenching for emitters and significantly enhance the upconversion luminescence.

To further understand the conceivable mechanism, we have studied the temporal behavior of the green emission (shown in Fig. 3(4)). Under direct downconversion excitation with 488 nm, the time trace of transition $^2H_{11/2}$ ($^4S_{3/2}$) → $^4I_{15/2}$ (~540 nm) was recorded, which directly reflects the de-population process of the emissive states. The decay curves can be reasonably well-fitted with a bi-exponential function. In all three models, the fast component τ_1 is around 10 μs, whereas the slow component τ_2 changes from 69.4 μs (model A), 54.7 μs (model B) to 36.8 μs (model C). Based on this result, we can perform qualitative analysis and gain an insight into the luminescence mechanism. The fast component τ_1, which is mainly contributed to by the outer layer $Er3^+$ ions, varies little among the three models, which simply manifests the fact that the distribution of the Er^{3+} ions in the outer layer is similar in all three models, whereas the long component τ_2 reflects more the properties of emitters in the inner shell.[11] The Er^{3+} concentration in model B is less than that in model C. A high doping level can cause luminescence quenching and the lifetime will be shortened. Therefore, the lifetime of model B is longer than that of model C. For the same Er^{3+} concentration, but different doping structure, *e.g.* models A and C, the lifetime of A is longer than that of C. We speculate that for model A, where the emitters are divided into different layers separated by an intermediate layer where only Yb^{3+} is doped, the excitation of the emitters of the inner layer cannot be effectively transferred to surface quenching centers *via* resonant energy transfer among emitters, extending the lifetime.

To further testify that the as-designed nanoparticle is beneficial to applications in biology/biomedicine, we have developed $NaYF_4$–Rose Bengal (UCP–RB) nanoconjugates to detect the improvement of singlet oxygen generation; a photodynamic therapy approach (see Fig. 4(1)). The singlet oxygen generation was confirmed by a chemical method using 1,3-diphenylisobenzofuran (DPBF) as a detector. DPBF irreversibly reacts with singlet oxygen causing a decrease in the absorption at 410 nm. Fig. 4(2) shows the decrease in the absorption at 410 nm in different samples. The slope of the curve is roughly proportional to the efficiency of generated singlet oxygen. Therefore, it is confirmed that the spatial separation of the emitter doping area can indeed greatly improve the biological behaviour of the rare-earth ion-doped nanoparticles (see Fig. S10† for detail).

This work was financially supported by NSF of china (11174277, 11004189, 10904142), the exchange program between CAS of China and KNAW of the Netherlands.

Notes and references

1 (*a*) F. Wang, D. Banerjee, Y. S. Liu, X. Y. Chen and X. G. Liu, *Analyst*, 2010, **135**, 1839; (*b*) P. Zhang, W. Steelant, M. Kumar and M. Scholfield, *J. Am. Chem. Soc.*, 2007, **129**, 4526; (*c*) Z. G. Chen, H. L. Chen, H. Hu, M. X. Yu, F. Y. Li, Q. Zhang, Z. Z. Zhou, T. Yi and C. H. Huang, *J. Am. Chem. Soc.*, 2008, **130**, 3023; (*d*) C. J. Carling, F. Nourmohammadian, J. C. Boyer and N. R. Branda, *Angew. Chem., Int. Ed.*, 2010, **49**, 3782; (*e*) G. F. Wang, O. Peng and Y. D. Li, *Chem.– Eur. J.*, 2010, **16**, 4923; (*f*) P. Zhang, S. Rogelj, K. Nguyen and D. Wheeler, *J. Am. Chem. Soc.*, 2006, **128**, 12410.
2 (*a*) Y. Wei, F. Q. Lu, X. R. Zhang and D. P. Chen, *Chem. Mater.*, 2006, **18**, 5733; (*b*) G. S. Yi and G. M. Chow, *Adv. Funct. Mater.*, 2006, **16**, 2324; (*c*) H. X. Mai, Y. W. Zhang, R. Si, Z. G. Yan, L. D. Sun, L. P. You and C. H. Yan, *J. Am. Chem. Soc.*, 2006, **128**, 6426; (*d*) J. Zhang, C. M. Shade, D. A. Chengelis and S. Petoud, *J. Am. Chem. Soc.*, 2007, **129**, 14834; (*e*) H. Schafer, P. Ptacek, K. Kompe and M. Haase, *Chem. Mater.*, 2007, **19**, 1396; (*f*) X. M. Liu, J. W. Zhao, Y. J. Sun, X. G. Kong and H. Zhang, *Chem. Commun.*, 2009, 6628.
3 J. C. Boyer and Frank C. J. M. Van Veggel, *Nanoscale*, 2010, **2**, 1417.
4 F. Wang, J. Wang and X. G. Liu, *Angew. Chem., Int. Ed.*, 2010, **49**, 7456.
5 F. Vetrone, R. Naccache, V. Mahalingam, C. G. Morgan and J. A. Capobianco, *Adv. Funct. Mater.*, 2009, **19**, 2924.
6 D. G. Yang, C. X. Li, G. G. Li, M. M. Shang and J. Lin, *J. Mater. Chem.*, 2011, **21**, 5923.
7 (*a*) S. Schietinger, T. Aichele, H. Q. Wang, T. Nann and O. Benson, *Nano Lett.*, 2010, **10**, 134; (*b*) H. Zhang, Y. J. Li, I. A. Ivanov, Y. Q. Qu, Y. Huang and X. F. Duan, *Angew Chem., Int. Ed.*, 2010, **49**, 2865.
8 F. Wang and X. G. Liu, *Chem. Soc. Rev.*, 2009, **38**, 976.
9 K. W. Kramer, D. Biner, G. Frei, H. U. Gudel, M. P. Hehlen and S. R. Luthi, *Chem. Mater.*, 2004, **16**, 1244.
10 J. W. Zhao, Y. J. Sun, X. G. Kong and H. Zhang, *J. Phys. Chem. B*, 2008, **112**, 15666.
11 Y. J. Sun, Y. Chen, L. J. Tian, Y. Yu, X. G. Kong and H. Zhang, *J. Lumin.*, 2008, **128**, 15.